Ocean Engineering 269 (2023) 113467

Contents lists available at ScienceDirect

Ocean Engineering

journal homepage: www.elsevier.com/locate/oceaneng

A vortex-induced vibration-based self-tunable airfoil-shaped piezoelectric energy harvester for remote sensing applications in water

Muhammad Hafizh [a], Asan G.A. Muthalif [a,*], Jamil Renno [a], M.R. Paurobally [a], Mohamed Sultan Mohamed Ali [b]

[a] Department of Mechanical and Industrial Engineering, Qatar University, Qatar
[b] Faculty of Electrical Engineering, Universiti Teknologi Malaysia, Johor Bahru, Malaysia

ARTICLE INFO

Handling Editor: Prof. A.I. Incecik

Keywords:
Piezoelectric energy harvesting
Vortex-induced vibration
Airfoil
Self-tuning
Pipeline industry
Rotating base

ABSTRACT

With growing innovations on the Internet of Things capabilities, automated monitoring and remote sensing applications have become important in the modern world. However, with thousands of distributed sensors and wireless communication routers, the power supply continues to be one of the main challenges for an efficient and sustainable operation. This paper deals with designing, developing, and testing a nonlinear airfoil-shaped piezoelectric energy harvester from flow-induced vibration. The harvester converts flow-induced vibration from water into electrical energy that can be conveniently stored and used to power smart remote sensors. A passive self-adjustable base compensates for the changing flow direction that can reduce the conversion efficiency of energy harvesters. Different beam substrate profiles were investigated for misalignment correction with thin airfoil profiles able to orient faster at higher misalignment angles. The airfoil-shaped piezoelectric energy harvester outperformed the conventional rectangular beams with equal volume with an additional inline mode observed for the same frequency range in low-velocity flow. The piezoelectric macro-fiber composite had an average RMS output of 132 mV for transverse oscillations in the absence of flow misalignment. Experimental studies have shown a performance reduction in both time and frequency domains between 50% and 60% for flow misalignment reaching up to 30°.

1. Introduction

Self-sufficient systems used for sensing and data collection are rapidly becoming ubiquitous throughout our lives (Erol-Kantarci and Mouftah, 2011; Ilyas, 2018; Quy et al., 2022; Zhang et al., 2012). This growing trend is directly feeding into big data analytics and the burgeoning concept of Smart Cities and Smart Infrastructure (Díaz et al., 2016). However, to fully realize the potential of such systems, power must be reliably supplied to them (Liu, 2012). Conventional methods of powering through batteries whose technology is well-established and well-developed unfortunately have a finite service life; they must be changed periodically, which requires additional resources for remote locations (Dutoit et al., 2005; Kamruzzaman and Alruwaili, 2022). Additionally, some processes require sensors to be embedded within the structure, which makes battery replacements impossible for underwater or underground applications. Remote sensing applications can wirelessly relay diagnostic information and data for asset integrity and monitoring (Bharani Baanu and Jinesh Babu, 2022; Khazaee et al., 2019; Zhou et al., 2016). Pipeline health monitoring presents an opportunity for self-sustaining systems when using remote sensing devices as power concerns become a limiting factor for mass deployment (Aramendia et al., 2019; Hallil et al., 2021; Kiziroglou et al., 2017).

Energy scavenging can be achieved through piezoelectric, electromagnetic, and electrostatic transduction methods, exploiting the abundant vibration and transducing it to electrical energy. The piezoelectric material converts vibration energy to electric energy. Additionally, piezoelectric energy harvesting (PEH) has been proven to provide excellent electromechanical energy conversion efficiency and high voltage that can be embedded in different structures (Safaei et al., 2019; Sodano et al., 2005; Yang et al., 2018). The maximum amount of energy converted by the piezoelectric material is usually when the host structure undergoes (linear) resonance at the system's natural frequency.

* Corresponding author.
E-mail addresses: mh1605936@qu.edu.qa (M. Hafizh), drasan@qu.edu.qa (A.G.A. Muthalif), jamil.renno@qu.edu.qa (J. Renno), mpaurobally@qu.edu.qa (M.R. Paurobally).
URL: https://sultan_alifke.utm.my (M.S. Mohamed Ali).

https://doi.org/10.1016/j.oceaneng.2022.113467
Received 25 May 2022; Received in revised form 19 October 2022; Accepted 18 December 2022
Available online 3 January 2023

However, in the linear vibration range, the resonance is narrow-banded due to the structure often being lightly damped. Since the vibration-based energy harvesters output maximum efficiency near the natural frequency, a slight deviation in the input source (or ambient surroundings) could drastically decrease the expected output. Nonlinear harvesters, on the other hand, utilize nonlinear vibration to broaden the bandwidth and thus make the harvester more robust and responsive to broadband or random vibrations (Ibrahim et al., 2017; Ibrahima et al., 2015; Zhang et al., 2019). Recent research results show that nonlinear energy harvesters can increase the frequency bandwidth. However, the amount of energy harvesters is less than what would be harvested by an equivalent linear harvester. Airfoil-based beams differ from conventional beams because the shape assists in both torsional and transverse vibration with self-aligning properties (Abdelkefi et al., 2012; Bao et al., 2019). An unrestricted rotational motion allows the piezoelectric energy harvester to always be directed to the incoming flow in misalignment scenarios, as shown in Fig. 1.

Energy harvesters have been successfully utilized to power smart wireless sensor nodes using a microprocessor, onboard memory, strain gauge, sensor signal conditioning, radio transceiver, and rechargeable battery (Shaikh and Zeadally, 2016; Wang et al., 2021; L. Wang et al., 2020). At a sampling rate of 10 Hz and 1 Hz, the average operating power was 900 and 90 μW, respectively, where a piezoelectric energy harvesting system could produce around 2000 μW at low-level vibration (Arms et al., 2005). The average power consumption of commercial sensor network nodes is in the range of 2 mW–12 mW using the IEEE 802.11 and the IEEE 802.15 standards for wireless networks (Gilbert and Balouchi, 2008). Energy harvesters can be used to convert the fluid kinetic energy of water into electrical energy using vortex-induced vibration (VIV) (Bearman, 2011; Gabbai and Benaroya, 2005; R Song et al., 2015; Sun et al., 2019a; J. Wang et al., 2020; Zhang et al., 2021). The literature highlighted that appropriately optimizing the resistances, and the bluff body sizing can improve the performance of piezo-hydro-elastic energy harvesters (Hafizh et al., 2021; Sun et al., 2019b; Wang et al., 2014). To maximize the scavenging of energy, the placement of piezoelectric layers on a cantilever beam should be optimally designed (Elahi et al., 2018; Takezawa et al., 2014). The amount of captured energy from the flow stream depends significantly on the local strain of the piezoelectric beam (Tan et al., 2021). Investigations have shown that for small piezoelectric arrays, the optimal location is close to the location of the maximum bending moment, but for large arrays, the optimal placement may not be at the point of the maximum bending moment (Cao et al., 2021; Sharma and Baredar, 2019). To compensate for piezoelectric energy harvesters' narrowband performance, nonlinearity can be introduced into the proposed design.

Bandwidth enhancement techniques using magnets have been investigated as viable alternatives to an effective broadband property but compromise the peak harvestable power output (Zhang et al., 2017). A novel self-aligning airfoil cantilever design introduces nonlinear energy harvesting properties that can increase conversion efficiency compared to conventional narrow-banded piezoelectric cantilever energy harvesters. Orrego et al. (2017) investigated the use of a passive self-aligning mechanism to compensate for changing wind directions in an inverted flag orientation, where outdoor testing results highlighted new opportunities for self-powered devices with fluctuating conditions and in low-speed regimes. The use of trailing guide wings has also been demonstrated to enhance performance in a wider velocity range (Gong et al., 2019). Verelest et al. (Verelst et al., 2014) demonstrated using a self-aligning base freely rotating on two bearings to remove the need for actively controlled mechanisms. A passive self-adjustable mechanism with an airfoil profile can be used to overcome the narrowband property of conventional cantilever piezoelectric beams due to random and broadband input flows (Manjock and Netzband, 2019; Netzband et al., 2020). Also, Lim et al. (2021) investigated a self-tunable wind energy harvester using transverse galloping mechanisms where the rotating base increased the output power for urban wind speeds. Tian et al. (2022) investigated a piezoaeroelastic and demonstrated that beyond the bifurcation point, the flutter performance can output a voltage of up to 29 V. The effects of structural parameters on the nonlinear aeroelastic response and energy harvesting performance were also experimentally investigated (Shan et al., 2020). There is still a gap in the research of piezoelectric energy harvesting with self-aligning behaviors that can compensate for losses in fluctuating flows, though some researchers have investigated the influence of the rotational motion present in vortex-induced vibration. Gong et al. (2020)investigated the use of vortex-induced vibration and subsequent swing amplitudes on a rotating base with a peak-peak output of 3.28 V in water. To the best of the author's knowledge, this paper presents the first study in airfoil-based hydrokinetic piezoelectric energy harvesting with computational simulations, experimental verification, and self-aligning behavior.

The remainder of the paper is organized as follows. Section 2 presents the analytical model and parameters of the proposed harvester, focusing on frequency-matching tuning. The computational domain, finite element, and experimental setup are explained in Section 3. Section 4 presented the results of the fluid-structure simulation interaction and the experiments for analytical model verification for a self-aligning airfoil-shaped energy harvester. The conclusions drawn from the results and this work are shown in Section 5.

2. Analytical model and parameters

Fig. 2(a) shows the physical model of the airfoil-shaped piezoelectric energy harvester connected to a circular bluff body. The cylindrical shape causes flow separation and causes the harvester assembly to oscillate perpendicular to the flow direction due to vortex-induced vibration. A carbon steel core is added to the internal structure of the bluff

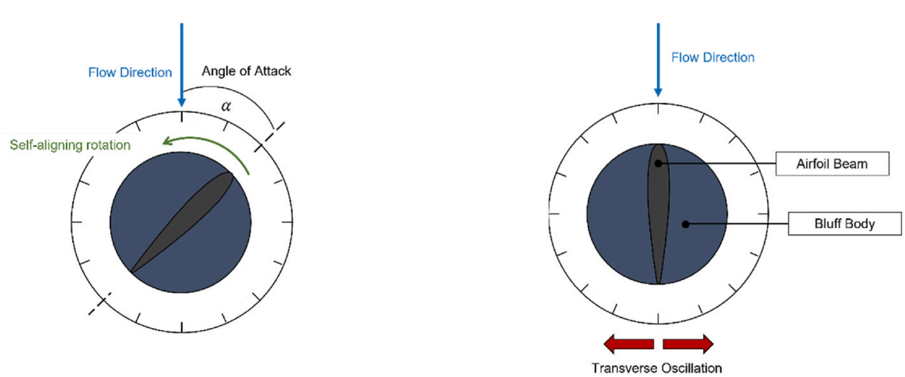

(a) (b)

Fig. 1. Self-Aligning Airfoil VIV Harvester; (a) Self-aligning rotation motion; (b) Aligned orientation with transverse oscillation.

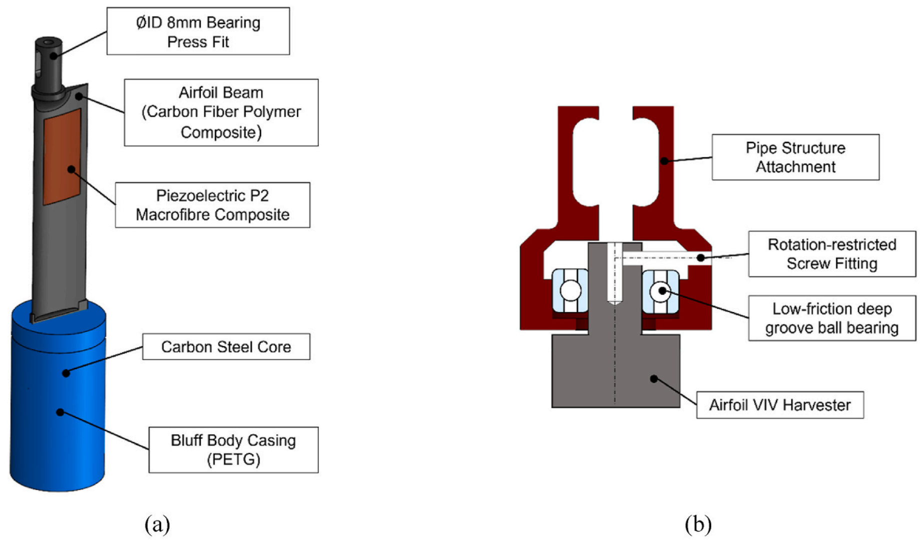

Fig. 2. Vortex-induced vibration energy harvester; (a) Airfoil Harvester schematic; (b) Self-aligning bearing holder schematic.

body to tune the energy harvester for low-velocity applications. A macrofibre composite (MFC) piezoelectric patch is attached to the airfoil beam and generates electricity from the mechanical strain of transverse vibration. The beam is mounted on a rotating base that is suspended by a bearing tolerance fit and allowed to rotate freely, as shown in Fig. 2(b). The airfoil beam utilized in the design is symmetrical to facilitate self-aligning properties without additional influence from the lift and drag of conventional airfoil shapes (Sarraf et al., 2010). A locking mechanism is added to stop the free rotation on the bearing to restrict the model. Table 1 lists the parameters and properties of the proposed energy harvester.

A discrete single degree of freedom (SDOF) model can be adopted to represent the first mode shape in this study. For the energy harvester undergoing periodic oscillations from vortex-induced vibration, a mass-spring-damper system can be modeled per unit time as Eq. (1):

$$M\ddot{x} + C\dot{x} + Kx + \Theta V_p = F_T(t) \qquad \text{Eq. 1}$$

Where M is the equivalent mass, C is the equivalent damping, and K is the equivalent stiffness. $\ddot{x}$, $\dot{x}$ and x represents the acceleration, velocity, and displacement of the oscillations, respectively. The effect with the electromechanical piezoelectric patch is modeled with Θ as the electromechanical coupling coefficient and V_p is the voltage produced. The current that is generated from the piezoelectric macrofibre composite with the term I, can be represented by Eq. (2) where C^S is the clamped capacitance value (Roundy and Wright, 2004; Xiao et al., 2015):

$$I(t) = \Theta\dot{x}(t) - C^S\dot{V}(t) \qquad \text{Eq. 2}$$

The transverse force F_T can be modeled as a forced vibration system using a two-parameter self-excitation model with in-phase and out-of-phase forces in Eq. (3) (Blevins, 2009):

Table 1
Parameters and variables for Airfoil Energy Harvester.

Symbol	Description	Value	Unit
D	Cylinder bluff-body diameter	*21*	*mm*
L	Airfoil substrate beam length	*60*	*mm*
H	Cylinder bluff-body height	*40*	*mm*
ρ_{beam}	Beam substrate density	*2770*	kg/m^3
$\rho_{cylinder}$	Cylinder bluff-body density	*5500*	kg/m^3
ρ_{piezo}	Active piezoelectric patch density	*7800*	kg/m^3
A_{2807}	2807-P2 piezoelectric active area	*196*	mm^2

$$F_T = \frac{\rho U^2 DL(C_{mv}\sin(2\pi ft) + C_{dv}\cos(2\pi ft))}{2} \qquad \text{Eq. 3}$$

Here, ρ represents the density of the flowing fluid, U is the freestream flow velocity, D is the diameter of the bluff body and L is the wetted span of the cylinder. C_{mv} represents the oscillating inertia coefficient whilst C_{dv} represents the oscillating negative damping coefficient. The cylinder oscillating frequency is represented by f. When the energy harvester is submerged underwater in the pipe array, the hydrodynamic effect of the water alters the SDOF model with added-mass parameters. This change to the equation of motion and, subsequently, the oscillation response and natural frequency of the overall harvester, as shown in Eq. (4):

$$(M + M_a)\ddot{x} + (\mathrm{C} + \mathrm{C_a} + C_p)\dot{x} + (\mathrm{K} + \mathrm{K_a} + K_p)x + \Theta V_p = F(t) \qquad \text{Eq. 4}$$

In linear energy harvesters, the resonant frequency ω_n is tuned to maximize the conversion efficiency near the peak amplitude displacement. In VIV applications, the energy harvester is also tuned at system resonance and is called 'synchronization' or 'lock-in region' (Jia et al., 2018; Mehmood et al., 2013; Williamson and Govardhan, 2004). For a submerged energy harvester placed in a large boundary, the assumption of low damping and no added stiffness can be adopted. However, these assumptions cannot be made in a pipeline system since the pipe boundary interaction would be significant enough to influence the overall system (Muthalif et al., 2022; Rodriguez et al., 2006; Xu et al., 2020). Thus, the subscript 'a' denotes added-mass properties, and 'p' is the pipe boundary interaction property. The derived ratios between air and underwater can be represented by Eqs. (5)–(7) where the subscript 'd' represents damped, and 'w' represents underwater:

$$\frac{\omega_{n,w}^2}{\omega_n^2} = \left(1 + \frac{K_a}{K}\right)\left(1 + \frac{M_a}{M}\right)^{-1} \qquad \text{Eq. 5}$$

$$\frac{\omega_{d,w}^2}{\omega_d^2} = \left(\frac{1 - \zeta_w^2}{1 - \zeta^2}\right)\left(1 + \frac{K_a}{K}\right)\left(1 + \frac{M_a}{M}\right)^{-1} \qquad \text{Eq. 6}$$

$$\frac{\zeta_w}{\zeta} = \left(1 + \frac{C_a}{C}\right)^2\left(1 + \frac{K_w}{K}\right)^{-1}\left(1 + \frac{M_w}{M}\right)^{-1} \qquad \text{Eq. 7}$$

Synchronization occurs when the shedding frequency of the vortices behind the bluff body is equivalent to the structural natural frequency of the energy harvester. Therefore, tuning the energy harvester to the desired freestream velocity is important in the design process. The calculation can be approximated by using the Strouhal number that can describe the oscillating mechanism shown in Eq. (8):

$$St = \frac{f_s D}{U_\infty} \quad \text{Eq. 8 (a)}$$

$$St = 0.1853 + 0.0261 \bullet \left[-0.9 \bullet \left(log\left(\frac{Re}{1.6 \times 10^3}\right)\right)\right] \quad \text{Eq. 8 (b)}$$

$$Re = \frac{\rho U_\infty D}{\mu} \quad \text{Eq. 9}$$

Where Re in Eq. (9) represents the Reynolds number valid and the Strouhal number approximation of the vortex shedding valid for the range $Re = 1.6 \times 10^3 - 1.5 \times 10^5$ (Norberg, 2003). The density and dynamic viscosity of the fluid is represented by ρ and μ, respectively. The freestream velocity is represented by U_∞ and bluff body diameter by D.

3. Setup

3.1. Computational fluid-structure interaction

Modeling the viscous and inertial forces of the fluid interaction was performed using a computational fluid dynamics (CFD) simulation. The domain setup consisted of three regions; the body; a deformable internal zone and an external zone as shown in Fig. 3. A two-dimensional setup on ANSYS Fluent v.2021R2 CFD software modeled the response of vortex-induced vibration on the bluff body and airfoil. A bluff body simulation was performed to model the lift and drag coefficients that cause the periodic oscillations in the energy harvester system. In contrast, the airfoil simulation modeled the response of the self-aligning mechanism to oncoming fluid flow. Airfoil simulations took advantage of adaptive meshing properties from the deformable internal zone to compensate for various misalignment angles. A second-order spatial discretization setting was adopted with implicit transient formulation with a $k - \omega$ SST turbulence model (Menter, 1994). The CFD solver utilized SIMPLE algorithm with a 2nd order $k - \omega$ transport equation (ANSYS Inc, 2021). The time step of 0.002s with 15 iterations per time step over a total 20s simulation time demonstrated a good vortex-shedding response for the cylinder and resolution for time comparison in airfoil rotation.

This CFD simulation was carried out using the authors' previous setup having performed a mesh dependency study and validating lift coefficients with values obtained from the literature (Hafizh et al., 2021; Muthalif et al., 2021). The mesh generated in the domain was initially adjusted for inflation around the bluff body and the y^+ value kept below unity to ensure adequate resolution and the same process was repeated for the airfoil boundary. In literature, a domain size of 40Dx20D was sufficient to model turbulence and VIV without boundary interaction (Aramendia et al., 2018; Fang and Han, 2011; Khan and Ibrahim, 2018; Zheng et al., 2020). The boundary of interest was placed 10D downstream from the velocity inlet to facilitate a good flow development. A non-slip boundary condition was used for the top and bottom walls. With a 5% blockage ratio, the impact of boundary conditions in the flow field can be sufficiently diminished (Zdravkovich, 1990). The average static reference pressure outlet was set to 0Pa.

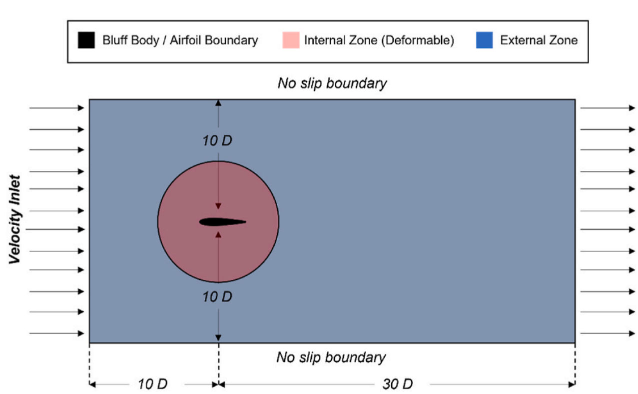

Fig. 3. Computational fluid dynamics domain setup.

The force coefficients and saved parameters from the CFD simulations were then linked to a finite element analysis (FEA) model to evaluate the electromechanical behavior of the piezoelectric energy harvester. The structural response of the vortex-induced vibration on the structure was also modeled on ANSYS Academic v.2021R2. For modeling and simulation in literature, the response of the vortex-induced vibration is modeled after forced response inputs of lift and drag coefficients (Blevins, 2009). The FEA simulation used in Fig. 2(a) was clamped at the circular bearing connection and force coefficients generated from the bluff body generated the response. The piezoelectric macrofibre composite properties of 2814-P2 (SmartMaterials, n.d.) were integrated with the material properties in the simulation to extract voltage output from mechanical strain. The results of the simulation were compared to previous work with good convergence (Ali et al., 2021; Erturk and Inman, 2008; Kuang and Zhu, 2019). The constitutive equation of piezoelectric materials expressed in stress-charge form is expressed as (SmartMaterials, n.d.):

$$\begin{Bmatrix} \{T\} \\ \{D\} \end{Bmatrix} = \begin{bmatrix} [c^E] & [e] \\ [e]^T & -[\varepsilon^S] \end{bmatrix} \begin{Bmatrix} \{S\} \\ \{E\} \end{Bmatrix} \quad \text{Eq. 10}$$

Where $\{T\}$ represents the stress, $\{D\}$ the electric flux density, $[c^E]$ elasticity at a constant electric field, $[e]$ piezoelectric stress, $[\varepsilon^S]$ dielectric matrix for a constant mechanical strain, $\{S\}$ elastic strain vector, and $\{E\}$ is the electric field intensity matrix. The material properties of the anisotropic piezoelectric macrofibre composite modeled after Smart Materials P2 (d_{31} effect) are shown in Table 2.

3.2. Experimental setup

The experimental setup to validate the experimental energy harvesting properties of the energy harvester was tested on an open water channel setup, as shown in Fig. 4. The authors' have previously utilized the setup in energy harvesting from vortex-induced vibration experiments (Muthalif et al., 2022). The setup was run on an Armstead's open channel water tank module with an adjustable water level and velocity by adjusting the gate and valve, respectively. The pipe-submerged energy harvester was placed 3 m from the water inlet to facilitate a developed flow in the channel. A T-beam secured the harvester clamped to the top of the setup and allowed for free rotation to model misalignment flow within the open channel. The data acquisition used a sampling frequency of 5000 Hz, and the time domain results were then exported into Fast Fourier transform (FFT) with a 0.2 Hz difference with a Hanning window. Experimental results were measured over 1 min, where the amplitude function of the frequency domain was averaged using energy distribution for each unit frequency. The energy average

Table 2
Modeled properties of MFC P2.

Material Property	Coefficient	Value
Stiffness (10^9 Pa)	$\overline{c}^E_{11} = \overline{c}^E_{22}$	168
	$\overline{c}^E_{21}$	110
	$\overline{c}^E_{31} = \overline{c}^E_{32}$	99.9
	$\overline{c}^E_{33}$	123
	$\overline{c}^E_{44}$	28.8
	$\overline{c}^E_{55} = \overline{c}^E_{66}$	30.1
Relative Permittivity	$\varepsilon_{11} = \varepsilon_{22}$	1902
	ε^S_{33}	1850
Piezoelectric constants	e_{31}	−10
	e_{33}	2.59
	e_{15}	0.1

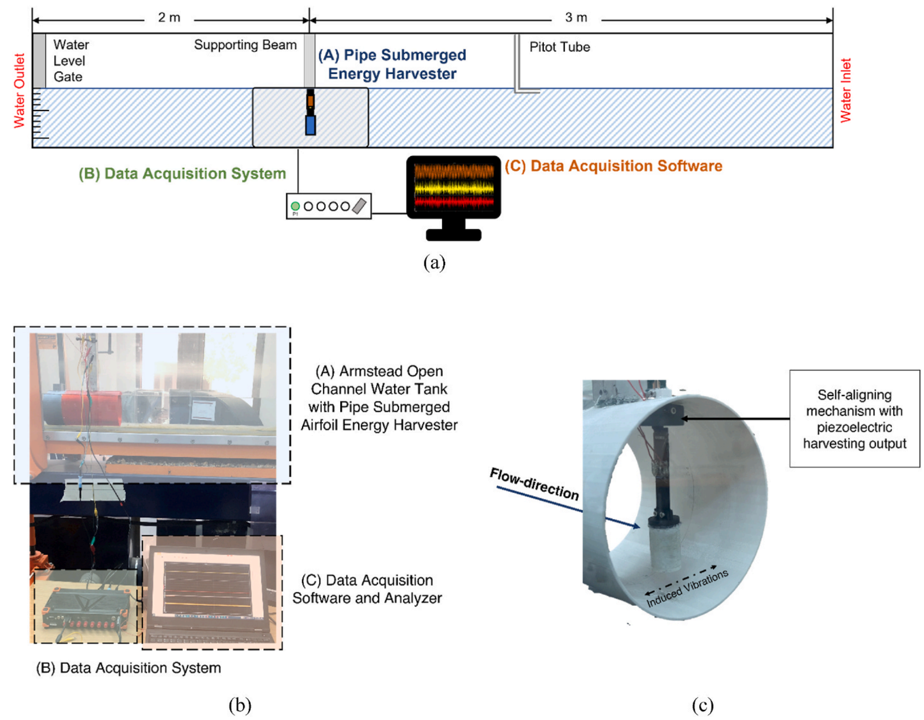

Fig. 4. Experimental Setup; (a) schematic; (b) energy harvester module with data acquisition experimental setup; (c) pipe submerged cross-section.

calculates the averages of the squared values of all values, like the root mean square (RMS).

4. Results

4.1. Computational fluid-structure interaction

The analysis of a self-aligning VIV harvester examines the effect of the flow direction and the effect of rotation on the overall property of energy harvesting. The computational domain and finite element setup in the previous section are used to simulate the behavior of an airfoil beam under different angles of attack, α. The methodology for modeling and optimization of the energy harvester can be seen in Fig. 5 where the main sections are divided between computational fluid dynamics (CFD); finite element analysis (FEA); and fluid-structure interaction (FSI).

In FEA, shape optimization studies were conducted on different airfoil structures. Because the harvester will primarily be utilized for low-velocity applications, the sizing of the airfoil is tuned to fit the first mode in the 1–10 Hz frequency requirement. Here, the selected airfoil shapes with a symmetric structure were selected as NACA0015 and NACA0024 for their slim profile and symmetric airfoil shape. Larger profiles will increase the natural frequency for the transverse mode and result in a higher cut-in velocity and smaller synchronization region (Lau et al., 2004). The structure's natural frequency was recorded for the different beam shapes, and a rectangular control beam of an identical natural frequency to NACA0015 was also simulated for a control parameter to compare, as shown in Fig. 6.

The frequency response of NACA0015 within a specified frequency range highlights the two main modes observable through vortex-induced vibration; transverse and inline (Blevins and Coughran, 2009; Muthalif et al., 2021; Qian-bei et al., 2019; Seyed-Aghazadeh et al., 2019; Taheri et al., 2021). One of the main advantages of submerged vibration-based energy harvesters is the ability to take advantage of both frequencies whilst not having any moving parts. Compared to a rectangular beam of equal mass and volume to NACA0015 in Fig. 6, an additional mode is present. Also, the voltage output of the airfoil beam is shown to have generated a higher output for the first transverse mode. This may be possible due to the non-uniform shape of the beam causing higher strains in deflections, also seen in the literature (Karadag et al., 2021; Mohamed et al., 2021; Muthalif and Nordin, 2015).

Next, the CFD simulated the layer separation caused by the vortices forming behind the bluff body that led to the periodic oscillation of VIV. The value of the Strouhal number from the vortex shedding is calculated from Eq. (8), but the frequency of vortex shedding results obtained was slightly lower than the expected value, causing a slight shift in the oscillation frequency. As a result of this shift, utilizing FSI underperforms the energy harvesting properties since the structure does not experience theoretical resonance. Therefore, the velocity of the flow was readjusted to conform with the structural frequency using the modified value of the Strouhal number. Finally, the self-aligning property of the airfoil is then simulated for the beam shapes rectangular, NACA0015 and NACA0024. In the CFD simulations, the velocity and pressure differences around the airfoil were observed to have changed while the self-aligning properties were in motion; this was also highlighted by other simulations seen in the literature (Tian et al., 2022). During misalignment in Fig. 7(a), visible turbulence forms behind the airfoil when measuring the velocity and pressure differences around the airfoil. With a low rotational stiffness (in low-friction ceramic bearings), the airfoil can be oriented with the incoming flow in Fig. 7(b) until levelled, where a streamline forms behind the airfoil before being separated.

The results CFD results for the different alignment durations were compared for the different angles of attack shown in Fig. 8. This study was carried out to investigate the effects of alignment for different beam profiles. A clear relationship can be seen between the sizing of the airfoil where the slimmer profile of the NACA0015 self-aligns faster than NACA0024 from 15° to 90° misalignment with more significant disparity at larger angles. Interestingly, for flow misalignment angles below 60° the rectangular beam performed better than NACA0015. However, at larger angles, NACA0015 could align itself much faster than the other profiles and therefore was used in the experimental setup.

4.2. Experimental results

The pipe submerged energy harvesting module placed inside the

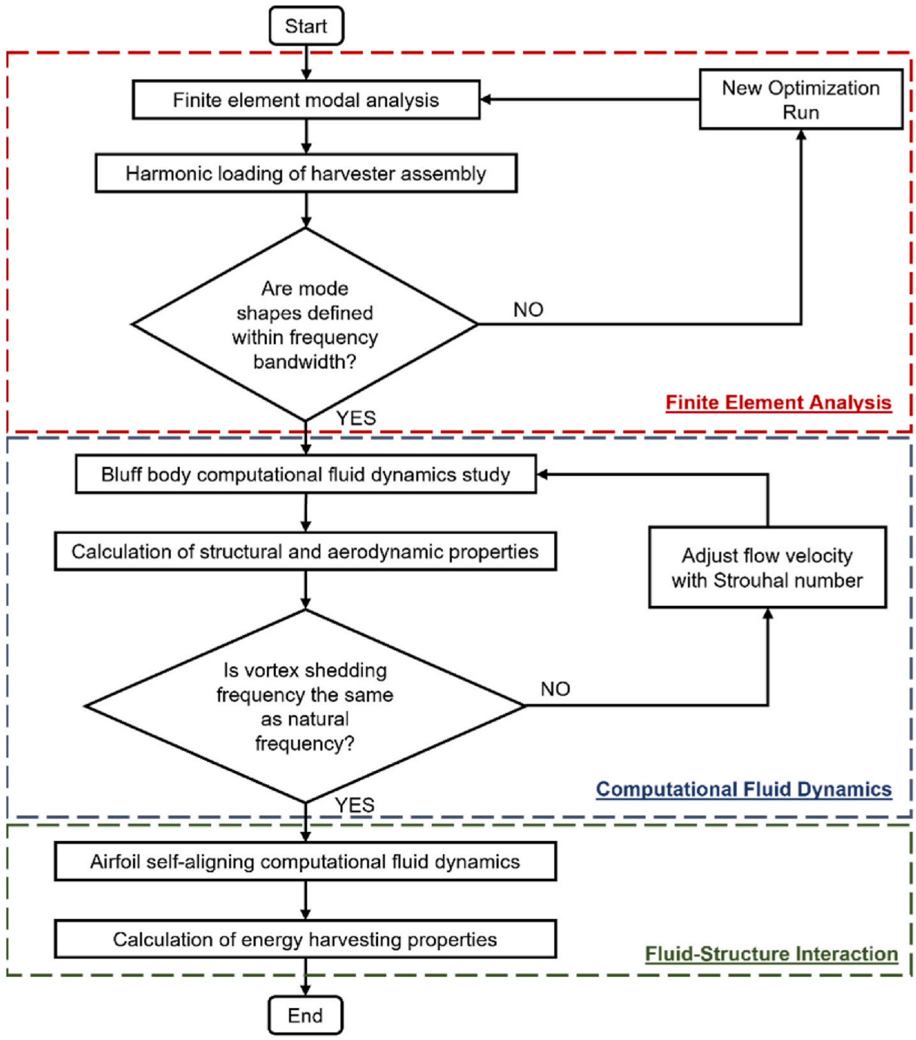

Fig. 5. Simulation and optimization study flowchart.

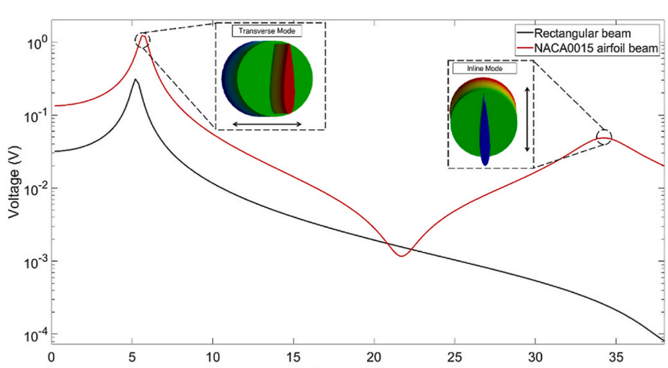

Fig. 6. NACA0015 airfoil energy harvester mode shapes.

water channel setup was evaluated over different misalignment angles for the NACA0015 airfoil. The averaged signal comparison between the different misalignment angles is highlighted in the time domain shown in Fig. 9 and the frequency domain in Fig. 10. Only misalignment angles up to 30° were taken during the experiment as larger angles within the allocated water channel changed drastically and did not provide sufficient flow development. The voltage output signals and the corresponding RMS values in Fig. 9 highlighted the conversion efficiency loss of 39%–58%, with the greatest interval drop seen at 10° misalignment.

The transverse mode that is expected from conventional cantilever beam piezoelectric energy harvesters is shown to be present at around 9 Hz in the frequency domain. The increase in natural frequency in the experiment compared to preliminary testing is done in the air resulting from the interaction of boundary and medium towards pipe-submerged conditions in the water. The added-mass effects and the effect of the pipe change the overall stiffness and damping properties that affect the energy harvester module (Muthalif et al., 2022; Rodriguez et al., 2006). In Fig. 10, a lower mode shape is visible in the FRF signal near 1.7–1.8 Hz, which was not visible when impulse testing in the transverse mode. The authors believe that this mode shape appeared from the torsional mode that was not visible in the preliminary tests. Additionally, in conventional piezoelectric beams, the entire upper surface is clamped where the first transverse mode is visible. As a result, the boundary on the bearing connection can contribute to torsional modes when the rotation is restricted. Nevertheless, the effects of the misalignment on a flow-induced energy harvester are visible by the reduced maximum voltage output produced over the measured tests. Table 3 outlines the measured resonant frequency and the maximum voltage output from the mode shapes.

Overall, the resonant frequency did not change largely, but the maximum voltage was negatively affected, ranging from 6% to 24% for 10° to 30° misalignments, respectively. Conversely, the first mode demonstrated a similar behavior of peak voltage reduction at a more drastic level between 23% and 53% for 10° to 30° misalignment,

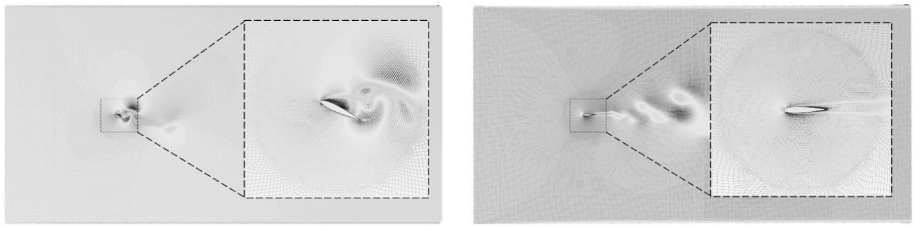

Fig. 7. Computational self-aligning behavior for NACA0015 at 30 ° misalignment.

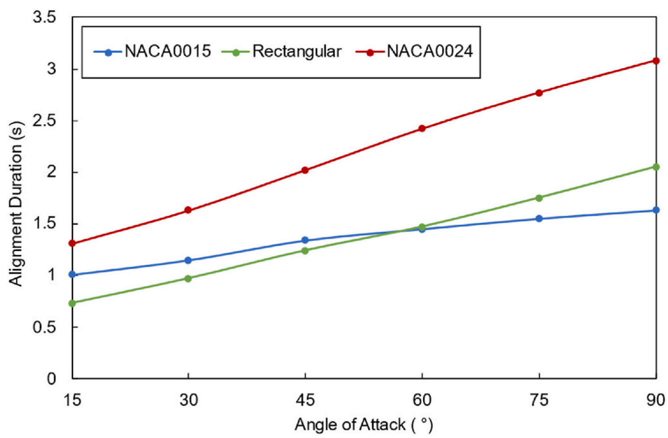

Fig. 8. Self-aligning property comparison.

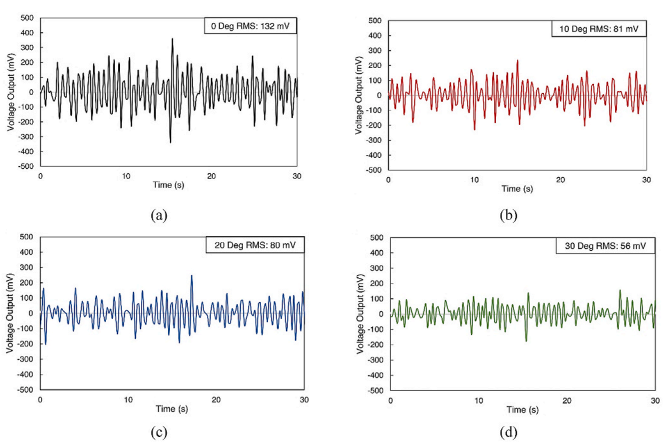

Fig. 9. Time-domain response of NACA0015 Airfoil energy harvester.

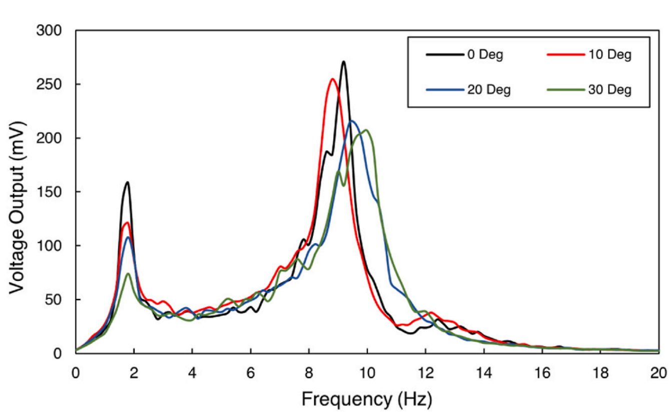

Fig. 10. Airfoil self-aligning experiment results for NACA0015.

Table 3
Captured mode shapes in experimental testing of NACA0015 airfoil.

Misalignment angle	Mode 1		Mode 2	
	$f_{resonance}$ (Hz)	V_{max} (mV)	$f_{resonance}$ (Hz)	V_{max} (mV)
0 deg	1.8	157	9.2	271
10 deg	1.8	121	8.8	255
20 deg	1.8	107	9.4	215
30 deg	1.8	74	10	207

respectively. A self-aligning rotating base mechanism still presents a gap in water flow mediums, with most of the work in literature focused on one-directional flow using rectangular beams only. Non-rotational clamped boundaries do not have performance losses since synchronization frequency is fixed to a single value. Therefore, there can be a tradeoff between the bandwidth performance of self-alignment with the higher peak output of narrowband piezoelectric energy harvesting. The lower voltage output of the current work can be explained by the pipe boundary condition increasing the damping properties through the 'added-mass' hydrodynamic effect; this was also highlighted by the results found by the author's previous work in submerged boundaries (Muthalif et al., 2022).

5. Conclusions

This paper proposed a self-aligning vortex-induced vibration-based piezoelectric energy harvester developed for remote sensing applications. A bluff body placed inside a moving fluid oscillates because the vortex-shedding frequency is synchronized with the system's natural frequency. A piezoelectric macrofibre composite attached to a beam generates electricity from mechanical strain. A rotating fixture mounted on the pipe accommodates the self-aligning behavior of the energy harvester to compensate for sudden changes in the flow direction. An analytical model was developed for a 1-DOF flow-induced vibration of the bluff body by accounting for the added hydrodynamic parameters of submerged bodies. The piezoelectric electromechanical coupling was then used to develop the finite element model in conjunction with computational fluid dynamics simulation to model fluid-structure interactions of vortex-induced vibration and misalignment. The findings of the study highlighted that:

- Airfoil-shaped beam can improve the response of piezoelectric energy harvesting in bandwidth-restricted applications with its non-uniform shape and self-tuning behavior which can be optimized for synchronization.
- Thin symmetric profiles (NACA0015) realign faster than larger profiles from uniform flow and can overcome large flow misalignments (above 60°) faster than conventional rectangular beams.
- Airfoil-shaped beams can take advantage of dual-mode synchronization at lower frequencies compared to a rectangular beam with an experimental RMS output of 132 mV.
- Non-tunable configurations exhibit significant drops in conversion efficiency by up to 50% for only 30° misalignments, are detrimental

to the harvesting efficiency and shift the transverse synchronization frequency.

The findings demonstrated that a self-aligned mechanism has excellent properties for application in open water channels and pipe-submerged channels that can be used to power remote sensing applications. Symmetric airfoil profiles with a freely rotating base introduce a passive mechanism for compensating flow directional variations. The use of advanced modeling and simulation techniques can reduce the time to market if suitably used. Also, additive manufacturing technologies and materials can be readily scaled and designed to power monitoring and diagnostic systems for pipe flow applications.

CRediT authorship contribution statement

Muhammad Hafizh: Methodology, Formal analysis, Investigation, Data curation, Writing – original draft, Writing – review & editing. **Asan G.A. Muthalif:** Conceptualization, Methodology, Validation, Funding acquisition, Project administration, Supervision, Visualization, Writing – review & editing. **Jamil Renno:** Validation, Writing – review & editing, Project administration. **M.R. Paurobally:** Validation, Writing – review & editing, Project administration. **Mohamed Sultan Mohamed Ali:** Validation, Writing – review & editing.

Declaration of competing interest

The authors declare that they have no known competing financial interests or personal relationships that could have appeared to influence the work reported in this paper.

Data availability

Data will be made available on request.

Acknowledgement

This work was partially supported by Qatar University - International Research Collaboration Grant no. IRCC-2020-017 and National Priorities Research Program Grant no. NPRP 11S–1220 – 170112. The findings achieved herein are solely the responsibility of the authors. Open Access funding provided by the Qatar National Library.

References

Abdelkefi, A., Nayfeh, A.H., Hajj, M.R., 2012. Modeling and analysis of piezoaeroelastic energy harvesters. Nonlinear Dynam. 67, 925–939. https://doi.org/10.1007/s11071-011-0035-1.

Ali, A., Muthalif, A.G.A., Renno, J., 2021. Broadband vibration energy harvesting from a non-deterministic system: performance of different piezoelectric patch shapes. Mater. Res. Express 8, 25702. https://doi.org/10.1088/2053-1591/abe063.

ANSYS Inc, 2021. ANSYS FLUENT User's Guide. Cannonsburg.

Aramendia, I., Fernandez-Gamiz, U., Guerrero, E.Z., Lopez-Guede, J.M., Sancho, J., 2018. Power control optimization of an underwater piezoelectric energy harvester. Appl. Sci. 8 https://doi.org/10.3390/app8030389.

Aramendia, I., Saenz-Aguirre, A., Boyano, A., Fernandez-Gamiz, U., Zulueta, E., 2019. Oscillating U-Shaped body for underwater piezoelectric energy harvester power optimization. Micromachines. https://doi.org/10.3390/mi10110737.

Arms, S.W., Townsend, C.P., Churchill, D.L., Galbreath, J.H., Mundell, S.W., 2005. Power management for energy harvesting wireless sensors. Smart Struct. Mater. 2005 Smart Electron. MEMS, BioMEMS Nanotechnol. 5763, 267–275. https://doi.org/10.1117/12.600302, 10.1117/12.600302.

Bao, C., Dai, Y., Wang, P., Tang, G., 2019. A piezoelectric energy harvesting scheme based on stall flutter of airfoil section. Eur. J. Mech. B Fluid 75, 119–132. https://doi.org/10.1016/j.euromechflu.2018.11.019.

Bearman, P.W., 2011. Circular cylinder wakes and vortex-induced vibrations. J. Fluid Struct. 27, 648–658. https://doi.org/10.1016/j.jfluidstructs.2011.03.021.

Bharani Baanu, B., Jinesh Babu, K.S., 2022. Smart water grid: a review and a suggestion for water quality monitoring. Water Supply 22, 1434–1444. https://doi.org/10.2166/WS.2021.342.

Blevins, R.D., 2009. Models for vortex-induced vibration of cylinders based on measured forces. J. Fluid Eng. 131 https://doi.org/10.1115/1.3222906.

Blevins, R.D., Coughran, C.S., 2009. Experimental investigation of vortex-induced vibration in one and two dimensions with variable mass, damping, and Reynolds number. J. Fluids Eng. Trans. ASME 131, 1012021–1012027. https://doi.org/10.1115/1.3222904.

Cao, Y., Cao, D., He, G., Ge, X., Hao, Y., 2021. Vibration analysis and distributed piezoelectric energy harvester design for the L-shaped beam. Eur. J. Mech. Solid. 87, 104214 https://doi.org/10.1016/j.euromechsol.2021.104214.

Díaz, M., Martín, C., Rubio, B., 2016. State-of-the-art, challenges, and open issues in the integration of Internet of things and cloud computing. J. Netw. Comput. Appl. 67, 99–117. https://doi.org/10.1016/J.JNCA.2016.01.010.

Dutoit, N.E., Wardle, B.L., Kim, S.-G., 2005. Desin considerations for MEMS-scale piezoelectric mechanical vibration energy harvesters. Integrated Ferroelectrics 71, 121–160. https://doi.org/10.1080/10584580590964574.

Elahi, H., Eugeni, M., Gaudenzi, P., 2018. A review on mechanisms for piezoelectric-based energy harvesters. Energies. https://doi.org/10.3390/en11071850.

Erol-Kantarci, M., Mouftah, H.T., 2011. Wireless sensor networks for cost-efficient residential energy management in the smart grid. IEEE Trans. Smart Grid 2, 314–325. https://doi.org/10.1109/TSG.2011.2114678.

Erturk, A., Inman, D.J., 2008. A distributed parameter electromechanical model for cantilevered piezoelectric energy harvesters. J. Vib. Acoust. 130 https://doi.org/10.1115/1.2890402.

Fang, Y., Han, Z., 2011. Numerical experimental research on the hydrodynamic performance of flow around a three dimensional circular cylinder. Appl. Mech. Mater. 90–93, 2778–2781. https://doi.org/10.4028/www.scientific.net/AMM.90-93.2778.

Gabbai, R.D., Benaroya, H., 2005. An overview of modeling and experiments of vortex-induced vibration of circular cylinders. J. Sound Vib. 282, 575–616. https://doi.org/10.1016/j.jsv.2004.04.017.

Gilbert, J.M., Balouchi, F., 2008. Comparison of energy harvesting systems for wireless sensor networks. Int. J. Autom. Comput. 5, 334–347. https://doi.org/10.1007/s11633-008-0334-2.

Gong, Y., Shan, X., Hu, H., Xie, T., Yang, Z., 2020. Vortex-induced swing (VIS) motion for energy harvesters and flowmeters. Appl. Phys. Lett. 117 https://doi.org/10.1063/5.0011899.

Gong, Y., Shan, X., Luo, X., Pan, J., Xie, T., Yang, Z., 2019. Direction-adaptive energy harvesting with a guide wing under flow-induced oscillations. Energy 187, 115983. https://doi.org/10.1016/j.energy.2019.115983.

Hafizh, M., Muthalif, A.G.A., Renno, J., Paurobally, M.R., Arab, M.A., Bahadur, I., Ouakad, H., 2021. A hybrid piezoelectric-electromagnetic nonlinear vibration energy harvester excited by fluid flow. Compt. Rendus Mec. 349, 65–81. https://doi.org/10.5802/crmeca.74.

Hallil, H., Dejous, C., Hage-Ali, S., Elmazria, O., Rossignol, J., Stuerga, D., Talbi, A., Mazzamurro, A., Joubert, P.Y., Lefeuvre, E., 2021. Passive resonant sensors: trends and future prospects. IEEE Sensor. J. 21, 12618–12632. https://doi.org/10.1109/JSEN.2021.3065734.

Ibrahim, D.S., Muthalif, A.G.A., Nordin, N.H.D., Saleh, T., 2017. Comparative study of conventional and magnetically coupled piezoelectric energy harvester to optimize output voltage and bandwidth. Microsyst. Technol. 23, 2663–2674. https://doi.org/10.1007/s00542-016-3066-1.

Ibrahima, D.S., Muthalif, A.G.A., Saleh, T., 2015. A piezoelectric based energy harvester with magnetic interactions: modelling and simulation. Adv. Mater. Res. 1115, 549–554. https://doi.org/10.4028/WWW.SCIENTIFIC.NET/AMR.1115.549.

Ilyas, M., 2018. Wireless sensor networks for smart healthcare. 1st Int. Conf. Comput. Appl. Inf. Secur. ICCAIS. https://doi.org/10.1109/CAIS.2018.8442038, 2018.

Jia, J., Shan, X., Upadrashta, D., Xie, T., Yang, Y., Song, R., 2018. Modeling and analysis of upright piezoelectric energy harvester under aerodynamic vortex-induced vibration. Micromachines 9, 667. https://doi.org/10.3390/mi9120667.

Kamruzzaman, M.M., Alruwaili, O., 2022. Energy efficient sustainable wireless body area network design using network optimization with smart grid and renewable energy systems. Energy Rep. 8, 3780–3788. https://doi.org/10.1016/J.EGYR.2022.03.006.

Karadag, C.V., Ertarla, S., Topaloglu, N., Okyar, A.F., 2021. Optimization of beam profiles for improved piezoelectric energy harvesting efficiency. Struct. Multidiscip. Optim. 63, 631–643. https://doi.org/10.1007/s00158-020-02714-0.

Khan, N.B., Ibrahim, Z., 2018. Numerical investigation of vortex-induced vibration of an elastically mounted circular cylinder with One-degree of freedom at high Reynolds number using different turbulent models. Proc. Inst. Mech. Eng. Part M J. Eng. Marit. Environ. 233, 443–453. https://doi.org/10.1177/1475090217751992.

Khazaee, M., Rezaniakolaie, A., Moosavian, A., Rosendahl, L., 2019. A novel method for autonomous remote condition monitoring of rotating machines using piezoelectric energy harvesting approach. Sensors Actuators, A Phys. 295, 37–50. https://doi.org/10.1016/j.sna.2019.05.016.

Kiziroglou, M.E., Boyle, D.E., Wright, S.W., Yeatman, E.M., 2017. Acoustic power delivery to pipeline monitoring wireless sensors. Ultrasonics 77, 54–60. https://doi.org/10.1016/j.ultras.2017.01.017.

Kuang, Y., Zhu, M., 2019. Evaluation and validation of equivalent properties of macro fibre composites for piezoelectric transducer modelling. Compos. B Eng. 158, 189–197. https://doi.org/10.1016/j.compositesb.2018.09.068.

Lau, Y.L., So, R.M.C., Leung, R.C.K., 2004. Flow-induced vibration of elastic slender structures in a cylinder wake. J. Fluid Struct. 19, 1061–1083. https://doi.org/10.1016/j.jfluidstructs.2004.06.007.

Lim, Y.Y., Padilla, R.V., Unger, A., Barraza, R., Thabet, A.M., Izadgoshasb, I., 2021. A self-tunable wind energy harvester utilizing a piezoelectric cantilever beam with bluff body under transverse galloping for field deployment. Energy Convers. Manag. 245, 114559 https://doi.org/10.1016/J.ENCONMAN.2021.114559.

Liu, Y., 2012. Wireless sensor network applications in smart grid: recent trends and challenges. Int. J. Distributed Sens. Netw. https://doi.org/10.1155/2012/492819, 2012.

Manjock, A., Netzband, S., 2019. Drift stability of HyStOH semi-submersible supported by airfoil shaped structures. J. Phys. Conf. Ser. 1222 https://doi.org/10.1088/1742-6596/1222/1/012025.

Mehmood, A., Abdelkefi, A., Hajj, M.R., Nayfeh, A.H., Akhtar, I., Nuhait, A.O., 2013. Piezoelectric energy harvesting from vortex-induced vibrations of circular cylinder. J. Sound Vib. 332, 4656–4667. https://doi.org/10.1016/j.jsv.2013.03.033.

Menter, F.R., 1994. Two-equation eddy-viscosity turbulence models for engineering applications. AIAA J. 32, 1598–1605. https://doi.org/10.2514/3.12149.

Mohamed, K., Elgamal, H., Kouritem, S.A., 2021. An experimental validation of a new shape optimization technique for piezoelectric harvesting cantilever beams. Alex. Eng. J. 60, 1751–1766. https://doi.org/10.1016/J.AEJ.2020.11.024.

Muthalif, A.G., Hafizh, M., Renno, J., Paurobally, M.R., 2022. A hybrid piezoelectric-electromagnetic energy harvester from vortex-induced vibrations in fluid-flow; the influence of boundary condition in tuning the harvester. Energy Convers. Manag. 256, 115371 https://doi.org/10.1016/j.enconman.2022.115371.

Muthalif, A.G.A., Hafizh, M., Renno, J., Paurobally, M.R., 2021. An enhanced hybrid piezoelectric–electromagnetic energy harvester using dual-mass system for vortex-induced vibrations. JVC/Journal Vib. Control 27, 2848–2861. https://doi.org/10.1177/10775463211041875.

Muthalif, A.G.A., Nordin, N.H.D., 2015. Optimal piezoelectric beam shape for single and broadband vibration energy harvesting: modeling, simulation and experimental results. Mech. Syst. Signal Process. 54, 417–426. https://doi.org/10.1016/j.ymssp.2014.07.014.

Netzband, S., Schulz, C.W., Abdel-Maksoud, M., 2020. Self-aligning behaviour of a passively yawing floating offshore wind turbine. Ship Technol. Res. 67, 15–25. https://doi.org/10.1080/09377255.2018.1555986.

Norberg, C., 2003. Fluctuating lift on a circular cylinder: review and new measurements. J. Fluid Struct. https://doi.org/10.1016/S0889-9746(02)00099-3.

Orrego, S., Shoele, K., Ruas, A., Doran, K., Caggiano, B., Mittal, R., Kang, S.H., 2017. Harvesting ambient wind energy with an inverted piezoelectric flag. Appl. Energy 194, 212–222. https://doi.org/10.1016/j.apenergy.2017.03.016.

Qian-bei, Y., Liu, G.R., Ju-bao, L., Liu, G.Z., min, L., Ri-zhi, D., 2019. Analyses of fluid-solid coupling dynamics of elastic tubes vibrating in cross flows. Eur. J. Mech. Solid. 73, 248–259. https://doi.org/10.1016/j.euromechsol.2018.09.004.

Quy, V.K., Hau, N. Van, Anh, D. Van, Quy, N.M., Ban, N.T., Lanza, S., Randazzo, G., Muzirafuti, A., 2022. IoT-enabled smart agriculture: architecture, applications, and challenges, 2022 Appl. Sci. 12, 3396. https://doi.org/10.3390/APP12073396. Page 3396 12.

Rodriguez, C.G., Egusquiza, E., Escaler, X., Liang, Q.W., Avellan, F., 2006. Experimental investigation of added mass effects on a Francis turbine runner in still water. J. Fluid Struct. 22, 699–712. https://doi.org/10.1016/j.jfluidstructs.2006.04.001.

Roundy, S., Wright, P.K., 2004. A piezoelectric vibration based generator for wireless electronics. Smart Mater. Struct. 13, 1131–1142. https://doi.org/10.1088/0964-1726/13/5/018.

Safaei, M., Sodano, H.A., Anton, S.R., 2019. A review of energy harvesting using piezoelectric materials: state-of-the-art a decade later (2008-2018). Smart Mater. Struct. 28, 113001 https://doi.org/10.1088/1361-665X/ab36e4.

Sarraf, C., Djeridi, H., Prothin, S., Billard, J.Y., 2010. Thickness effect of NACA foils on hydrodynamic global parameters, boundary layer states and stall establishment. J. Fluid Struct. 26, 559–578. https://doi.org/10.1016/j.jfluidstructs.2010.02.004.

Seyed-Aghazadeh, B., Edraki, M., Modarres-Sadeghi, Y., 2019. Effects of boundary conditions on vortex-induced vibration of a fully submerged flexible cylinder. Exp. Fluid 60, 38. https://doi.org/10.1007/s00348-019-2681-x.

Shaikh, F.K., Zeadally, S., 2016. Energy harvesting in wireless sensor networks: a comprehensive review. Renew. Sustain. Energy Rev. 55, 1041–1054. https://doi.org/10.1016/j.rser.2015.11.010.

Shan, X., Tian, H., Cao, H., Feng, J., Xie, T., 2020. Experimental investigation on a novel airfoil-based piezoelectric energy harvester for aeroelastic vibration. Micromachines 11. https://doi.org/10.3390/MI11080725.

Sharma, P.K., Baredar, P.V., 2019. Analysis on piezoelectric energy harvesting small scale device – a review. J. King Saud Univ. Sci. 31, 869–877. https://doi.org/10.1016/j.jksus.2017.11.002.

SmartMaterials, n.d. Macro Fiber Composite - MFC, Sensor, Energy Harvester Energy Harvesting Systems Piezo Powering and Instrumentation Engineering Services.

Sodano, H.A., Inman, D.J., Park, G., 2005. Comparison of piezoelectric energy harvesting devices for recharging batteries. J. Intell. Mater. Syst. Struct. 16, 799–807. https://doi.org/10.1177/1045389X05056681.

Song, R., Shan, X., Li, J., Xie, T., Sun, Q., 2015. A piezoelectric energy harvester with vortex induced vibration. In: 2015 Symposium on Piezoelectricity, Acoustic Waves, and Device Applications (SPAWDA), pp. 322–325. https://doi.org/10.1109/SPAWDA.2015.7364499.

Sun, W., Zhao, D., Tan, T., Yan, Z., Guo, P., Luo, X., 2019a. Low velocity water flow energy harvesting using vortex induced vibration and galloping. Appl. Energy 251, 113392. https://doi.org/10.1016/J.APENERGY.2019.113392.

Sun, W., Zhao, D., Tan, T., Yan, Z., Guo, P., Luo, X., 2019b. Low velocity water flow energy harvesting using vortex induced vibration and galloping. Appl. Energy 251, 113392. https://doi.org/10.1016/j.apenergy.2019.113392.

Taheri, E., Zhao, M., Wu, H., Munir, A., 2021. Energy harvesting from inline vibration of an elastically mounted circular cylinder in oscillatory flow. Ocean Eng. 239, 109694 https://doi.org/10.1016/j.oceaneng.2021.109694.

Takezawa, A., Kitamura, M., Vtanabe, S.L., Silva, E.C.N., 2014. Design methodology of piezoelectric energy-harvesting skin using topology optimization. Struct. Multidiscip. Optim. 49, 281–297. https://doi.org/10.1007/s00158-013-0974-x.

Tan, T., Zuo, L., Yan, Z., 2021. Environment coupled piezoelectric galloping wind energy harvesting. Sensors Actuators, A Phys. 323, 112641 https://doi.org/10.1016/j.sna.2021.112641.

Tian, H., Shan, X., Cao, H., Xie, T., 2022. Enhanced performance of airfoil-based piezoaeroelastic energy harvester: numerical simulation and experimental verification. Mech. Syst. Signal Process. 162, 108065 https://doi.org/10.1016/j.ymssp.2021.108065.

Verelst, D.R.S., Larsen, T.J., Van Wingerden, J.W., 2014. Wind tunnel tests of a free yawing downwind wind turbine. J. Phys. Conf. Ser. 555 https://doi.org/10.1088/1742-6596/555/1/012103.

Wang, G., Li, P., Wen, Y., Luo, Z., Han, T., Ji, X., 2021. Self-powered ultra-low-power low-threshold synchronous circuit for weak piezoelectric energy harvesting. Sensors Actuators, A Phys. 322, 112632 https://doi.org/10.1016/j.sna.2021.112632.

Wang, J., Geng, L., Ding, L., Zhu, H., Yurchenko, D., 2020. The state-of-the-art review on energy harvesting from flow-induced vibrations. Appl. Energy. https://doi.org/10.1016/j.apenergy.2020.114902.

Wang, J., Ran, J., Zhang, Z., 2014. Energy harvester based on the synchronization phenomenon of a circular cylinder. Math. Probl Eng. https://doi.org/10.1155/2014/567357, 2014.

Wang, L., Zhao, L., Luo, G., Zhao, Y., Yang, P., Jiang, Z., Maeda, R., 2020. System level design of wireless sensor node powered by piezoelectric vibration energy harvesting. Sensors Actuators, A Phys. 310, 112039 https://doi.org/10.1016/j.sna.2020.112039.

Williamson, C.H.K., Govardhan, R., 2004. Vortex-induced vibrations. Annu. Rev. Fluid Mech. 36, 413–455. https://doi.org/10.1146/annurev.fluid.36.050802.122128.

Xiao, H., Wang, X., John, S., 2015. A dimensionless analysis of a 2DOF piezoelectric vibration energy harvester. Mech. Syst. Signal Process. 58, 355–375. https://doi.org/10.1016/j.ymssp.2014.12.008.

Xu, W., Yang, M., Wang, E., Sun, H., 2020. Performance of single-cylinder VIVACE converter for hydrokinetic energy harvesting from flow-induced vibration near a free surface. Ocean Eng. 218, 108168 https://doi.org/10.1016/j.oceaneng.2020.108168.

Yang, Z., Zhou, S., Zu, J., Inman, D., 2018. High-performance piezoelectric energy harvesters and their applications. Joule 2, 642–697. https://doi.org/10.1016/J.JOULE.2018.03.011.

Zdravkovich, M.M., 1990. Conceptual overview of laminar and turbulent flows past smooth and rough circular cylinders. J. Wind Eng. Ind. Aerod. 33, 53–62. https://doi.org/10.1016/0167-6105(90)90020-D.

Zhang, L.B., Abdelkefi, A., Dai, H.L., Naseer, R., Wang, L., 2017. Design and experimental analysis of broadband energy harvesting from vortex-induced vibrations. J. Sound Vib. 408, 210–219. https://doi.org/10.1016/j.jsv.2017.07.029.

Zhang, L.B., Dai, H.L., Abdelkefi, A., Wang, L., 2019. Experimental investigation of aerodynamic energy harvester with different interference cylinder cross-sections. Energy 167, 970–981. https://doi.org/10.1016/j.energy.2018.11.059.

Zhang, M., Zhang, C., Abdelkefi, A., Yu, H., Gaidai, O., Qin, X., Zhu, H., Wang, J., 2021. Piezoelectric energy harvesting from vortex-induced vibration of a circular cylinder: effect of Reynolds number. Ocean Eng. 235, 109378 https://doi.org/10.1016/j.oceaneng.2021.109378.

Zhang, Y., Li, X., Zhang, S., Zhen, Y., 2012. Wireless sensor network in smart grid: applications and issue. Proc. 2012 World Congr. Inf. Commun. Technol. WICT 1204–1208. https://doi.org/10.1109/WICT.2012.6409258, 2012.

Zheng, M., Han, D., Gao, S., Wang, J., 2020. Numerical investigation of bluff body for vortex induced vibration energy harvesting. Ocean Eng. 213, 107624 https://doi.org/10.1016/j.oceaneng.2020.107624.

Zhou, K., Fu, C., Yang, S., 2016. Big data driven smart energy management: from big data to big insights. Renew. Sustain. Energy Rev. 56, 215–225. https://doi.org/10.1016/J.RSER.2015.11.050.